Gravity as Temporal Geometry II: Experimental Signatures of Quantum Temporal Geometry
Paper II in the Time-First Gravity Series

Adam Snyder
Independent Researcher

August 16, 2025

Abstract

We recast GR in lapse-first variables and derive two clock-native observables: (i) a sign-definite flux→redshift-drift template, and (ii) a general visibility kernel that bounds the two-point correlator of lapse fluctuations. We introduce no extra propagating degrees of freedom and make no timeline claims. We provide analysis-ready estimators, null tests, and sensitivity bounds: laboratory runs serve as pipeline validations with synthetic injections; astrophysical campaigns (e.g., Galactic SN triggers) enable pre-registered template searches. The paper is self-contained: Appendix 7 derives the flux law from EF/Vaidya, and Appendix 7 lists the ADM degree-of-freedom ledger (two TT modes).

Keywords: General relativity, quantum gravity, optical clocks, atom interferometry, gravitational phase noise, time geometry

Scope & claims (conservative). (1) All results are within semiclassical GR; no extra polarizations or propagating scalars are introduced. (2) Laboratory runs are *validation only* via *synthetic (software) injections* (sign and strict $1/r$ software scaling). (3) "Bounds" denote *ideal analysis sensitivity* (exact filters with measured $S_y(f)$); actual measurements are limited by current technology. No detection timelines are asserted. (4) Remarks on horizons/information are moved to an outlook as speculative templates, not claims.

1 Introduction and summary

We cast gravity as *time geometry*: the lapse $\mathcal{N} = e^{\Phi}$ is primary, the shift $\boldsymbol{\omega}$ carries rotation and mass currents, and spatial geometry evolves via the ADM constraints [1] in these variables. This choice makes many observables *clock-native*.

Terminology. Here "quantum temporal geometry" refers to semiclassical temporal phase fluctuations of the lapse (constraint-projected metric/stress fluctuations within GR), not an additional propagating scalar or beyond-GR degree of freedom.

Positioning. The results here live entirely within semiclassical GR: we quantify and bound the **quantum temporal phase** seen by clocks (via C_Φ, S_Φ) as a constraint-projected effect of quantized matter and linearized gravitons. This does not obviate the need for a full quantum-gravity theory; it provides a **testable, low-energy sector** that any candidate theory must reproduce.

Gauge honesty. We work lapse-first (Φ primary) and allow non-zero shift for dynamics; the diagonal gauge is a convenience, not a law. PG/EF maps and equivalence are detailed in Appendix 7.

Section 2 recalls a crisp classical result (Flux→Redshift–Drift). Sections 3–4 develop quantum consequences that are (i) fully within GR at the semiclassical level and (ii) directly testable as phase/visibility effects. The derivations needed here are rederived in Appendices 7–7; Paper I [2] provides additional pedagogy.

Why this matters (bounds-first). Expressed in lapse-first variables, many gravitational observables are directly clock-native. This affords clean *bounds*—not guaranteed detections—because (i) the spherical flux→drift template is sign-locked and $1/r$, and (ii) interferometric visibilities map linearly to the two-point function of $\delta\Phi$. The contribution here is a conservative, GR-equivalent pipeline: analysis-ready templates, null tests, and sensitivity estimates that existing platforms can use to set limits.

2 Classical anchor: Flux→Redshift–Drift

Notation and units

Signature $(-,+,+,+)$; c is explicit. Areal radius r satisfies $4\pi r^2$ area. Fractional frequency $y \equiv \ln(\nu_\infty/\nu_r)$. We use one-sided spectra: $S_\Phi(\Omega)$ with units [s], and $S_y(f)$ with units [Hz^{-1}]. All Fourier conventions and filter functions $F(\Omega)$ are stated where used.

In diagonal spherical gauge,

$$\mathrm{d}s^2 = -\mathrm{e}^{2\Phi}\,\mathrm{d}t^2 + \mathrm{e}^{-2\Phi}\,\mathrm{d}r^2 + r^2\mathrm{d}\Omega^2, \qquad \mathcal{N} = \mathrm{e}^{\Phi}, \tag{1}$$

In spherical symmetry, the observable far-field relation is most transparently obtained in EF/Vaidya form and reads[1]

$$\partial_t\Phi(t,r) \simeq -\frac{G}{c^4}\,\frac{L(t)}{r} \qquad \text{(outgoing flux; sign flips for ingoing)}, \tag{2}$$

where $L(t)$ is the luminosity crossing the sphere of areal radius r. Equation (2) is the operational law we template against in data; Appendix 7 shows its derivation from EF/Vaidya and discusses how local stress-energy components map to $L(t)$.

Sign convention. Outgoing energy flux ($L > 0$) increases the exterior mass parameter, decreasing $A = e^{2\Phi} = 1 - \frac{2Gm}{rc^2}$ and thus Φ; therefore $\partial_t\Phi < 0$ (redshift). Conversely, ingoing flux yields $\partial_t\Phi > 0$ (blueshift). In EF/Vaidya, $L = -c^2\,dm/dv$ and $\partial_v\Phi = -(G/c^4)\,L/r$, consistent with Eq. (2).

Equivalently,

$$\frac{\mathrm{d}}{\mathrm{d}t}\ln\!\Big(\frac{\nu_\infty}{\nu_r}\Big) = \partial_t\Phi(t,r). \tag{3}$$

Appendix 7 reproduces (2) from EF/Vaidya [3] $m(v)$ with $A = \mathrm{e}^{2\Phi} = 1 - 2Gm/(rc^2)$, confirming classical GR equivalence.

[1] Rotation/frame dragging lives in the shift $\boldsymbol{\omega}$ (gravitomagnetism); a spatially uniform $\partial_t\Phi$ cannot generate a transverse B_g.

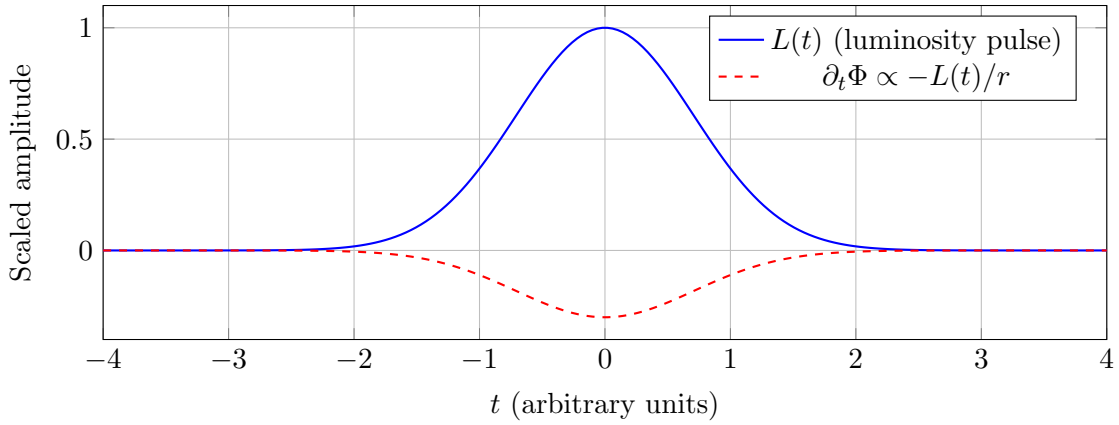

Figure 1: Flux→Redshift–Drift template: A toy Gaussian luminosity pulse $L(t)$ and the corresponding sign-definite redshift-drift prediction $\partial_t\Phi \propto -L(t)/r$ from Eq. (2). The template is phase-locked to the flux and provides a controlled experimental signature.

3 Temporal phase accumulation along worldlines

3.1 Worldline phase from the clock field

A massive system with rest energy E accumulates phase

$$\theta = \frac{1}{\hbar}\int E\,\mathrm{d}\tau = \frac{1}{\hbar}\int E\,\mathcal{N}\,\mathrm{d}t = \omega\int \mathrm{e}^{\Phi(t,\boldsymbol{x}(t))}\mathrm{d}t, \qquad \omega \equiv \frac{E}{\hbar}. \tag{4}$$

For small fluctuations $\Phi = \bar{\Phi} + \delta\Phi$ and fixed path ($\delta\Phi$ is the constraint-projected h_{00} of linearized GR, not a new propagating scalar; see Sec. 6),

$$\delta\theta \simeq \omega\int \delta\Phi(t)\,\mathrm{d}t. \tag{5}$$

For internal transitions replace $E\to\Delta E$ (optical clock: $\omega = \Delta E/\hbar$).

3.2 Visibility kernel (general path difference)

Consider a two-path interferometer with path indicator $f(t) = \pm 1$ on the two arms. The phase difference from (5) is

$$\Delta\theta = \omega\int f(t)\,\delta\Phi(t)\,\mathrm{d}t. \tag{6}$$

Assuming Gaussian $\delta\Phi$ with correlator $C_\Phi(t,t') = \langle\delta\Phi(t)\delta\Phi(t')\rangle$, the ensemble-averaged fringe visibility is

Visibility law.

$$\mathcal{V} = \exp\left[-\frac{1}{2}\,\omega^2\iint f(t)\,C_\Phi(t,t')\,f(t')\,\mathrm{d}t\,\mathrm{d}t'\right]. \tag{7}$$

This is the *time-first* analogue of phase diffusion: every system is a clock of Φ, with strength set by ω.

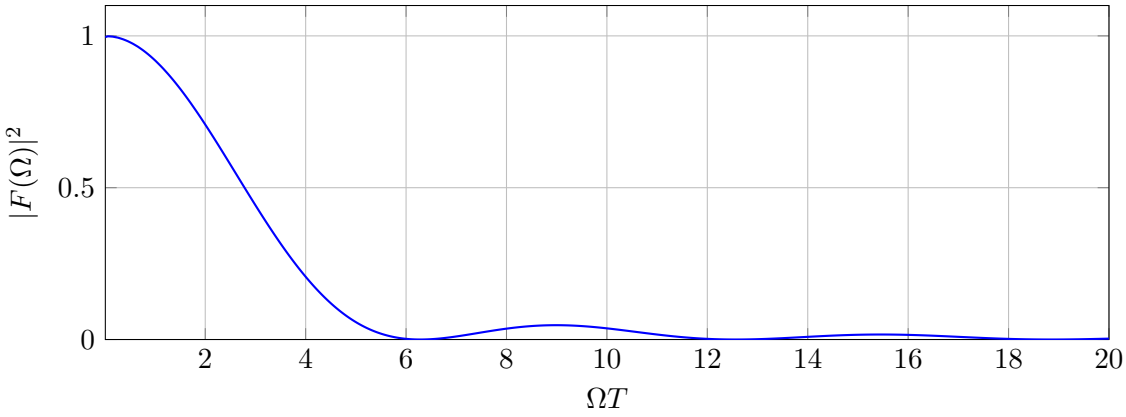

Figure 2: Visibility filter function for a rectangular timing window: $|F(\Omega)|^2 = \left(\frac{2\sin(\Omega T/2)}{\Omega}\right)^2$ for a simple Ramsey/Mach–Zehnder interrogation of duration T. The sinc^2 envelope determines which frequency components of $S_\Phi(\Omega)$ contribute most to visibility loss via Eq. (8).

Universality of temporal decoherence. Equation (7) shows $-\ln \mathcal{V} \propto \omega^2$, with $\omega = E/\hbar$ the system's clock frequency. Thus *every* system couples to Φ in proportion to its energy: macroscopic superpositions (large E) decohere rapidly, while mesoscopic superpositions can retain visibility. This provides a natural, observer-native explanation of the quantum-to-classical transition via temporal phase noise rather than spatial localization.

3.3 Spectral form and decoherence rate

For stationary noise, $C_\Phi(t,t') = C_\Phi(t-t')$ with one-sided spectral density $S_\Phi(\Omega)$. We use *one-sided* power spectral densities $S_\Phi(\Omega)$, $S_y(f)$ with units $[S_\Phi] = \mathrm{s}$, $[S_y] = \mathrm{Hz}^{-1}$. If $f(t)$ is a sequence of plateaus/pulses (Mach–Zehnder with separation time T), then

$$-\ln \mathcal{V} = \frac{\omega^2}{2} \int_0^\infty \frac{\mathrm{d}\Omega}{2\pi}\, S_\Phi(\Omega)\, |F(\Omega)|^2\,, \qquad F(\Omega) = \int f(t)\, e^{i\Omega t} \mathrm{d}t. \tag{8}$$

For long interrogation and low-frequency dominated S_Φ, the dephasing rate is

$$\Gamma_\phi \simeq \frac{\omega^2}{2}\, S_\Phi(0) \quad \text{(Markovian limit)}. \tag{9}$$

Turning visibility into a bound. In the Markovian limit, $-\ln \mathcal{V} \simeq \frac{1}{2}\omega^2 S_\Phi(0)\, T$, hence

$$S_\Phi(0) \;\lesssim\; \frac{2|\ln \mathcal{V}|}{\omega^2 T}. \tag{10}$$

For $T = 1\,\mathrm{s}$ and an optical transition $\omega/2\pi = 10^{15}\,\mathrm{Hz}$, a 1% (resp. 0.1%) visibility loss corresponds to $S_\Phi(0) \lesssim 5 \times 10^{-34}\,\mathrm{s}$ (resp. $5 \times 10^{-35}\,\mathrm{s}$).

Origin of C_Φ (semiclassical GR). There is no extra scalar graviton. In lapse-first gauge, Φ is fixed by the Hamiltonian constraint; projecting linearized metric fluctuations and stress-tensor fluctuations onto the clock frame induces an effective correlator C_Φ for $\delta\Phi$. Operationally, C_Φ combines (i) vacuum TT modes mapped into h_{00} by the constraints and (ii) stress-tensor fluctuations of the environment (stochastic gravity [4, 5]). The visibility law, Eq. (7), is therefore a re-expression of standard GR predictions in clock-native variables.

Scenario	L [W]	r [m]	$\lvert\partial_t\Phi\rvert$ [s^{-1}]
Sgr A* bright flare	10^{29}	1.2×10^{13}	6.9×10^{-29}
XRB outburst	10^{31}	1.0×10^{10}	8.3×10^{-24}
Galactic SN (neutrino)	3×10^{45}	3×10^{20}	8.3×10^{-20}
Lab lamp (control)	10^{4}	10	8.3×10^{-42}
Pulsed lab source	10^{14} (1 MJ/10 ns)	10	8.3×10^{-32}

Table 1: Order-of-magnitude redshift-drift rates from various sources. Astrophysical events provide the strongest signals, while laboratory sources serve as controlled calibration standards. (XRB: X-ray binary; AGN: active galactic nucleus; SNEWS: SuperNova Early Warning System). *Remark:* The Galactic supernova line ($|\partial_t\Phi|\sim10^{-20}\,\mathrm{s}^{-1}$) is within roughly an order of current optical-clock stability, motivating coordinated campaigns when alerts occur.

4 Two levers for experiments

Units and spectral conventions. We use SI with $c,\hbar$ explicit and treat Φ as *dimensionless* ($N=e^{\Phi}$), so $\partial_t\Phi$ has units [s^{-1}]. For stationary noise, $C_\Phi(t-t')$ admits a one-sided PSD. With angular frequency Ω and measure $\int_0^\infty \frac{d\Omega}{2\pi}$, the one-sided $S_\Phi(\Omega)$ has units [**s**] and

$$-\ln\mathcal{V}=\frac{\omega^2}{2}\int_0^\infty\frac{d\Omega}{2\pi}\,S_\Phi(\Omega)\,|F(\Omega)|^2$$

is dimensionless as $|F(\Omega)|^2$ has units [s^2]. Equivalently, with ordinary frequency f (Hz) and measure $\int_0^\infty df$, the one-sided $S_\Phi(f)$ has units [$\mathbf{Hz}^{-1}$] with $S_\Phi(f)=S_\Phi(\Omega{=}2\pi f)/(2\pi)$. Clock fractional-frequency PSDs use $S_y(f)$ in [$\mathbf{Hz}^{-1}$].

The dimensional constant $G/c^4=8.262\times10^{-45}\,\mathrm{s}^2/(\mathrm{kg\,m})$ sets the scale for all effects.[2] Table 1 shows order-of-magnitude estimates for various astrophysical scenarios using $|\partial_t\Phi|\approx(G/c^4)\,L/r$.

4.1 Lever A: Controlled classical flux ($L(t)$) $\Rightarrow$ redshift drift

Place two co-located optical clocks at radius r and modulate a distant, high-power beam dump or lamp to generate a known $L(t)$. Then

$$\frac{\mathrm{d}}{\mathrm{d}t}\ln\!\Big(\frac{\nu_\infty}{\nu_r}\Big)=\partial_t\Phi(t,r)\approx-\frac{G}{c^4}\frac{L(t)}{r}\tag{11}$$

provides a *phase-locked* template against which to cross-correlate clock residuals. The prediction is sign-definite and $1/r$.

Optimal estimator and stacking. Model the data as $y(t)=-\lambda s(t)+n_y(t)$ with $s(t)=\int^t L(t')\,dt'$ and $\lambda=G/(c^4r)$. The GLS (or whitened matched filter) variance is

$$\mathrm{Var}(\hat\lambda)=\left[2\int_0^\infty\frac{|s(f)|^2}{S_y(f)}\,df\right]^{-1},\qquad s(f)=\frac{L(f)}{i2\pi f}.\tag{12}$$

Practical note. Since $s(f)=L(f)/(i2\pi f)$ concentrates power below the flare bandwidth, the estimator integrates in the sub-Hz band where $S_y(f)$ is lowest for state-of-the-art optical clocks. Stacking M flares increases the integral by M (hence $\mathrm{SNR}\propto\sqrt{M}$), and two-clock cross-correlation reduces uncorrelated noise by $\sqrt{2}$ while preserving the common gravitational signal.

[2] Using $G=6.674\times10^{-11}\,\mathrm{m}^3/(\mathrm{kg\,s}^2)$ and $c=2.998\times10^8\,\mathrm{m/s}$ to four significant figures.

Uncertainty propagation (nuisances). Let $\hat{\lambda}$ be estimated by GLS with variance $\mathrm{Var}_{\mathrm{stat}}(\hat{\lambda}) = \left[2\int_0^\infty |s(f)|^2/S_y(f)\,df\right]^{-1}$. Nuisance parameters enter as linearized fractional errors: range $r \to r(1+\epsilon_r)$, power calibration $L \to L(1+\epsilon_L)$, and PSD mis-model $S_y \to S_y(1+\epsilon_S)$. To first order,

$$\frac{\delta\hat{\lambda}}{\hat{\lambda}} \simeq -\epsilon_r - \epsilon_L + \mathcal{O}(\epsilon_S),$$

since $s(f) \propto L(f)/(i2\pi f)$ rescales with L. Thus

$$\mathrm{Var}_{\mathrm{tot}}(\hat{\lambda}) \;\approx\; \mathrm{Var}_{\mathrm{stat}}(\hat{\lambda}) \;+\; \hat{\lambda}^2\big(\sigma_r^2 + \sigma_L^2\big) \;+\; \Delta_S,$$

with σ_r, σ_L the fractional uncertainties on r and the absolute calibration of L, and Δ_S a (typically subdominant) contribution from PSD mis-modeling estimated by re-fitting under bracketed $S_y(f)$ curves. We report both $\mathrm{Var}_{\mathrm{stat}}$ and $\mathrm{Var}_{\mathrm{tot}}$.
Practical note. For laboratory tests, calibration systematics in r and L typically dominate over the statistical term $\mathrm{Var}_{\mathrm{stat}}(\hat{\lambda})$.

4.2 Lever B: Quantum fluctuations ($\delta\Phi$) $\Rightarrow$ visibility loss

Atom interferometer (Mach–Zehnder). With interrogation time T and effective frequency ω (internal splitting), the filter $F(\Omega)$ is the standard two-pulse kernel [6]; measuring $\mathcal{V}(T)$ places bounds on $S_\Phi(\Omega)$ through (8). A *driven* variant injects shot-noise dominated photon flux at controlled distance to imprint a calculable S_Φ via stress-tensor fluctuations.

Co-located optical clocks. Cross-correlate fractional frequency noise of two clocks [7, 8] at separation Δr while modulating $L(t)$ (classical) or operating in quiet conditions (quantum/stochastic). The former tests (11); the latter constrains $S_\Phi(0)$ via (9).

Optomechanical cat states. For a superposition $|L|+|R|$ separated primarily in *time spent* at different potentials, the off-diagonal decays as $\exp[-\Gamma_\phi t]$ with Γ_ϕ from (9). This isolates *temporal* (not spatial) decoherence [9].

Practical observer workflow. Measure $y(t) \equiv \ln(\nu_\infty/\nu_r)$ from two clocks at radius r. Obtain a contemporaneous luminosity proxy $L(t)$ for the nearby source. Fit the model $\dot{y}(t) = -\lambda L(t) + \sum_k a_k X_k(t) + n(t)$ with λ predicted as $G/(c^4 r)$ and regressors X_k for Doppler/instrumental terms. Verify sign and $1/r$ scaling across events.

4.3 Case study: Sgr A* pulsar vs. Galactic supernova

A Sgr A* flare with $L \sim 10^{29}\,\mathrm{W}$ over $\Delta t \sim 10^4\,\mathrm{s}$ at $r = 1.2 \times 10^{13}\,\mathrm{m}$ yields $\Delta\Phi \sim -6.9 \times 10^{-25}$, i.e. a fractional frequency step far below present pulsar timing. By contrast, a Galactic core-collapse SN with $L_\nu \sim 3 \times 10^{45}\,\mathrm{W}$ for $10\,\mathrm{s}$ at $r \sim 10\,\mathrm{kpc}$ gives $\Delta\Phi \sim 8 \times 10^{-19}$, motivating a clock-network [10] search template phase-locked to the neutrino burst.
Conclusion. Sgr A* pulsar timing during flares is conceptually clean but presently sub-threshold. A Galactic SN neutrino burst is an *operationally promising target of opportunity* for phase-locked template fitting and global clock-network cross-correlation (no timeline implied).

4.4 Sensitivity and feasibility (bounds-first)

Using Eq. (8) with the exact filter $|F(\Omega)|^2$ for a two-pulse sequence gives the Markovian bound (10), so $S_\Phi(0) \lesssim \frac{2|\ln V|}{\omega^2 T}$. For $T = 1\,\mathrm{s}$ and an optical $\omega/2\pi = 10^{15}\,\mathrm{Hz}$, resolving $\mathcal{V} \geq 0.99$ (resp. 0.999) gives $S_\Phi(0) \lesssim 5 \times 10^{-34}\,\mathrm{s}$ (resp. $5 \times 10^{-35}\,\mathrm{s}$).

Current technology context. Bounds from Eq. (10) are *ideal analysis limits* assuming isolation from technical and environmental noise. State-of-the-art optical comparisons achieve fractional frequency stability approaching $\sigma_y \sim 10^{-19}$ at $\tau = 1$ s [11], limited by measured $S_y(f)$ and sub-Hz gravity-gradient noise [11–13]. Near-term goals are therefore: (i) end-to-end *pipeline validation* with *synthetic (software) injections*, (ii) sign-locking and strict $1/r$ software scaling checks, and (iii) upper limits using the measured $S_y(f)$ and filter-weighted integrals.

In ground labs, the sub-Hz band is typically dominated by Newtonian gravity-gradient noise and technical phase noise; our protocol treats these as measured $S_y(f)$ inputs and reports *bounds* that are robust to non-white $S_\Phi(\Omega)$ via the filter-weighted integral.

Flux template: calibration vs. detection. The laboratory flux template $\dot{y}(t) = -\lambda L(t)$ with $\lambda = G/(c^4 r)$ is sign-definite and scales as $1/r$. For laboratory powers and $r \sim 5$–$20\,\mathrm{m}$ the implied signals are far below detectability; we therefore classify such runs as *pipeline validations using synthetic (software) injections*: recover the sign-locked template and verify *injected* $1/r$ scaling, and demonstrate the registered analysis on real noise. Astrophysical campaigns (e.g. a Galactic SN) should be treated as *template searches with pre-registered tests* yielding either a coefficient consistent with λ within uncertainties or an upper limit.

5 Implementation methods

5.1 Lever A: Controlled flux experimental protocol

Geometry and distance specification. r is the straight-line distance from the emitting source to the clock pair's midpoint. Keep the two clocks within $\ll r$ so both see the same $L(t)$. For lab tests, use $r \geq 5$–$10\,\mathrm{m}$ to keep near-field EM/thermal effects negligible.

Measuring $L(t)$ in practice.

- **Laboratory:** Place a calibrated, fast power meter (photodiode + integrating sphere) at the clock location to record $F(t)$ ($\mathrm{W/m^2}$). Compute $L(t) = 4\pi r^2 F(t)$. State the detector bandwidth ($\geq$ the source modulation bandwidth).
- **Astrophysical:** Use accepted proxies: for supernovae, neutrino counts/energies from SuperNova Early Warning System (SNEWS) 2.0 [14]/IceCube/Super-K to construct $L_\nu(t)$ (state the conversion used); for X-ray binary (XRB)/active galactic nucleus (AGN) flares, satellite photon flux in specified band with bolometric corrections noted.

Sign and alignment rule. Align $\dot{y}(t)$ and the **locally measured** $L(t)$. If $L(t)$ comes from a remote observatory stream, shift it by the light-travel time difference so it represents the flux at the clocks. The expected template is **zero-lag** after this alignment.

Shielding and null tests. Require: black baffles and IR shielding between source and clocks; Faraday shielding if the source drive current is large; temperature and magnetic monitors near the clocks. Mandate two nulls: (i) run with the source on but power dumped into a cold trap (no photons escaping), (ii) run with shutters closed but identical electrical drive on the source.

Clock configuration for cross-correlation. Two **independent** optical clocks and local oscillators (no shared LO) to improve SNR by $\sqrt{2}$. Record $y(t) = \ln(\nu_\infty/\nu_r)$ at $\geq 1\,\mathrm{Hz}$ with UTC/TAI time-tags. If clocks are separated, use stabilized fiber/White Rabbit/Two-Way Satellite Time and Frequency Transfer (TWSTFT) and state the transfer stability.

Exact analysis recipe.

1. Whiten $\dot{y}(t)$ by the measured one-sided $S_y(f)$.
2. Build $s(t) = \int^t L(t')\,dt'$; compute $s(f) = L(f)/(i2\pi f)$.
3. Estimate λ with GLS/matched filter; quote $\mathrm{Var}(\hat{\lambda}) = [2\int_0^\infty |s(f)|^2/S_y(f)\,df]^{-1}$.
4. Pre-register: (i) frequency band, (ii) vetoes, (iii) stacking rule (SNR $\propto \sqrt{M}$), (iv) pass/fail based on sign and strict $1/r$ scaling.

Demonstrating $1/r$ scaling. In lab: repeat at $r = \{5, 10, 20\}\,\mathrm{m}$. For astronomy: compare **different sources at known distances** (same instrument chain), since Earth-baseline differences are negligible relative to source distance.

5.2 Lever B: Quantum phase visibility protocol

Pulse sequence specification. The two most common $f(t)$: Ramsey and Raman Mach–Zehnder ($\pi/2$-π-$\pi/2$). For the standard two-pulse kernel [6], $F(\Omega) = \frac{2e^{i\Omega T/2}\sin(\Omega T/2)}{\Omega}$ giving $|F(\Omega)|^2 = (2\sin(\Omega T/2)/\Omega)^2$.

Reporting requirements. Quote $\mathcal{V}(T)$ with error bars and the **band-integrated** bound inferred via $-\ln\mathcal{V} = \frac{\omega^2}{2}\int_0^\infty S_\Phi(\Omega)|F(\Omega)|^2\,\frac{d\Omega}{2\pi}$. If presenting the Markovian $S_\Phi(0)$ bound, also provide the filter-weighted integral bound (more robust for non-white noise).

Noise budget components. List three contributors: Newtonian gravity-gradient (dominant $< 1\,\mathrm{Hz}$), photon shot/thermal stress-tensor, and TT vacuum fluctuations—plus standard lab sources (laser phase noise, vibration, BBR/magnetic shifts). Require a "source-off" baseline and subtraction.

5.3 Galactic supernova case study

Trigger and data window. Use SNEWS 2.0 as the trigger; record $\pm 6\,\mathrm{h}$ around the alert at $\geq 1\,\mathrm{Hz}$. Provide mapping from neutrino counts $\to L_\nu(t)$ (even as a range with priors).

Consortium requirements. Acceptable time-transfer methods: UTC/TAI traceability via GPS Common View (GPSCV), TWSTFT, or stabilized fiber. Each site must publish $S_y(f)$ and the whitening filter used.

Pre-registered test. A detection requires: correct sign, zero-lag (post-alignment), and $\lambda = G/(c^4 r)$ within error bars. Report a combined constraint if not detected.

5.4 Implementation warnings

Near-field contamination. Controlled-flux lab runs are **pipeline validations**, not physics detections. EM/thermal near-field couplings dwarf the gravitational signal and are handled by the nulls and shielding protocols above.

No new degrees of freedom. $\delta\Phi$ is the constraint-projected h_{00} from linearized GR. The "effective action" in Appendix B is a noise-kernel model, not a propagating scalar field.

6 Consistency: no extra DOF, GR equivalence

Time-first variables reorganize, but do not enlarge, GR. In ADM language, Φ (lapse) and $\boldsymbol{\omega}$ (shift) are Lagrange multipliers that enforce the Hamiltonian and momentum constraints; only the transverse-traceless tensor modes propagate in vacuum. The correlator C_Φ that enters (7) is not a new degree of freedom; it is the constrained, gauge-fixed projection of linearized metric fluctuations (plus stress-tensor fluctuations) onto the observer's clock.

Hence all experimental signatures described here are *re-expressions* of standard GR physics in clock-native variables, making them far more direct to compute and measure than traditional metric-based approaches.

6.1 Registered analysis and null tests

Pre-registration: (i) band of analysis; (ii) vetoes; (iii) stacking rule; (iv) pass/fail defined by sign and strict $1/r$ scaling (flux template) or by a pre-specified visibility threshold (phase bounds). **Exact steps (flux template):** whiten $\dot{y}(t)$ by measured $S_y(f)$; build $s(t) = \int^t L(t')dt'$ so $s(f) = L(f)/(i2\pi f)$; estimate λ with GLS/matched filter; quote variance $[2\int_0^\infty |s(f)|^2/S_y(f)\,df]^{-1}$. **Nulls:** (i) shuttered source with identical drive; (ii) cold power dump; (iii) time slides between sites; (iv) off-band analyses. **Outcome:** coefficient consistent with $\lambda = G/(c^4 r)$ within error bars, or an upper limit; for visibilities, a bound on $S_\Phi(\Omega)$ (Markovian and filter-weighted).

Pre-registration protocol for flux-template searches

1. **Band:** specify analysis band (e.g., $[0.01, 10]$ Hz).
2. **Vetoes:** define glitch vetoes (e.g., excursions $> 5\sigma$) and data-gap handling ($> 10\%$ window).
3. **Stacking:** state stacking rule (coherent sum across M events; SNR $\propto \sqrt{M}$).
4. **Success:** (a) correct sign, (b) $\hat{\lambda}$ within 2σ of $G/(c^4 r)$, (c) all null tests pass.
5. **Registry:** archive the protocol and parameter choices in a timestamped repository.

7 Outlook: horizons and temporal phase (speculative template)

Because Φ captures clock-rate warping, Eq. (2) ties exterior clock relaxation during evaporation to outgoing flux in a bookkeeping sense. A light-cone–peaked cross-correlation template for clock

residuals can be written for analog platforms; however, astrophysical temperatures make this unobservable today. We include this only as a *template* for future analog systems or small-BH scenarios; it is not used elsewhere in the paper and carries no claim of near-term detectability.

Appendix A: EF/Vaidya cross-check of the flux law

In EF (v, r) with $ds^2 = -(1 - 2Gm/rc^2)c^2dv^2 + 2c\,dv\,dr + r^2d\Omega^2$ and $T_{vv} = (dm/dv)/(4\pi r^2)$, the luminosity is $L = -c^2 dm/dv$ and $\partial_v \Phi = -(G/c^4)L/r$, reproducing (2).

Appendix B: ADM degree-of-freedom ledger (lapse-first)

In ADM form $ds^2 = -N^2dt^2 + \gamma_{ij}(dx^i + N^i dt)(dx^j + N^j dt)$ with $N = e^\Phi$ and $N^i = \omega^i$, the action yields the Hamiltonian and momentum constraints $\mathcal{H}_\perp \approx 0$ and $\mathcal{H}_i \approx 0$; N and N^i are Lagrange multipliers (no conjugate momenta). Linearizing about Minkowski and imposing TT gauge leaves only two tensor polarizations propagating; no scalar/vector mode propagates in vacuum. Thus our lapse-first variables reorganize GR but do not enlarge its dof.

Appendix C: Phenomenological quadratic kernel for C_Φ

We model the *two-point statistics* of the clock fluctuation $\delta\Phi$ with a quadratic *kernel* that reproduces the same correlator C_Φ used in (7) without introducing any propagating scalar degree of freedom. Formally,

$$\mathcal{S}^{(2)}[\,\delta\Phi\,] = \frac{1}{2}\int d\tau\, d^3x\, K(\tau, \mathbf{x})\, \delta\Phi(\tau, \mathbf{x})\, \delta\Phi(\tau, \mathbf{x}), \tag{13}$$

where the (nonlocal, positive) kernel K is fixed by the constrained projection of linearized GR and by stress-tensor fluctuations (stochastic gravity). This device is merely a Gaussian representation of C_Φ; **no new propagating mode** is implied. The propagating content remains exactly that of GR (two TT tensor modes), see Appendix 7.

Appendix D: Visibility kernel—derivation and filters

For Gaussian $\delta\Phi$ with zero mean, $\langle e^{i\Delta\theta}\rangle = \exp[-\frac{1}{2}\langle\Delta\theta^2\rangle]$, and $\Delta\theta = \omega\int f(t)\delta\Phi(t)\mathrm{d}t$ gives

$$-\ln\mathcal{V} = \frac{\omega^2}{2}\iint f(t)C_\Phi(t,t')f(t')\mathrm{d}t\,\mathrm{d}t'.$$

Common filters: (i) Ramsey: $f(t)$ is $+1$ then -1 with gap T; (ii) Mach–Zehnder: $f(t)$ is a pair of plateaus; (iii) spin-echo variants implement high-pass versions of $F(\Omega)$ in Eq. (8).

Non-ideal pulses. Use the *measured* drive $f_{\rm meas}(t)$ so $F(\Omega) = \int f_{\rm meas}(t)e^{i\Omega t}\,dt$. Finite rise/fall times reshape $|F(\Omega)|^2$; in low-band, step-like sequences this induces fractional corrections scaling as $\mathcal{O}\big((T_{\rm rise}/T)^2\big)$ (equivalently $\sim\int d\Omega\,(\Omega T_{\rm rise})^2|F(\Omega)|^2$). The matched filter and bounds remain valid without deconvolution.

Appendix E: Systematics and discriminants

The predicted flux→redshift–drift signature has several key discriminants that distinguish it from instrumental and astrophysical systematics:

Sign-locking. The sign of $\partial_t \Phi$ is definitively locked to the sign of $L(t)$: outgoing flux produces negative drift, ingoing flux produces positive drift. This provides a robust test against correlated noise sources.

Distance scaling. The effect scales precisely as $1/r$, verified by measuring the same source from different locations or comparing sources at known distances. This distinguishes the effect from local instrumental drifts and plasma propagation effects.

Cross-correlation analysis. The template correlation $\langle \dot{y}(t), L(t) \rangle$ should be maximized at zero lag with coefficient $\lambda = G/(c^4 r)$. Systematic effects typically produce different lag structures or distance-independent coefficients.

Regression framework. Standard analysis fits:

$$\dot{y}(t) = -\lambda L(t) + a_1 \dot{r}_{\mathrm{Doppler}}(t) + a_2 T_{\mathrm{plasma}}(t) + a_3 \delta f_{\mathrm{inst}}(t) + n(t) \tag{14}$$

where regressors account for Doppler velocity shifts, plasma dispersion variations, and instrumental frequency drifts. The gravitational signature should remain robust across this systematic removal.

Laboratory calibration. A pulsed source (1 MJ in 10 ns) at $r = 10$ m gives $|\dot{\Phi}| \sim 8 \times 10^{-32}$ s^{-1} and $\Delta\Phi \sim 8 \times 10^{-40}$. While far below detectability, this provides an end-to-end calibration: (1) inject a known $L(t)$, (2) recover the sign-locked template in software, and (3) verify the $1/r$ falloff by repeating at $r = 5, 10, 20$ m. Two co-located clocks demonstrate common-mode preservation under cross-correlation.
Operational role. While the pulsed-source signal is undetectable as physics, it *validates the entire pipeline*: template recovery in the presence of realistic noise, sign verification, and the $1/r$ scaling by moving the source. Success here demonstrates end-to-end readiness for astrophysical campaigns.

Source	$\lvert\partial_t \Phi\rvert$ [s^{-1}]	Status
Lab lamp (10 W @ 10 m)	$\sim 8 \times 10^{-42}$	Pipeline test (software)
Pulsed laser (1 MJ / 10 ns)	$\sim 8 \times 10^{-32}$	Pipeline test (software)
Galactic SN (proxy luminosity)	$\sim 8 \times 10^{-20}$	Network template search
Clock fractional stability (1 s)	$\sim 10^{-19}$ (ref. S_y)	Noise reference

Table 2: Comparison of flux-driven redshift-drift amplitudes to present measurement capability. Laboratory sources are 12–22 orders of magnitude below current clock stability and serve only for pipeline validation via *synthetic (software) signal injection*. Only astrophysical events approach measurable scales.

Appendix F: Quantum noise budget for $S_\Phi(\Omega)$

Vacuum TT modes. The constrained projection of linearized metric fluctuations yields $S_\Phi^{\mathrm{vac}}(\Omega) = \alpha(\Omega)\, S_h^{\mathrm{TT}}(\Omega)$, with α fixed by the Hamiltonian constraint kernel (typically extremely small in the lab band).
Stress-tensor fluctuations (shot/thermal). For a radiative flux L at distance r, $S_\Phi^{\mathrm{shot}}(\Omega) \sim (G/c^4 r)^2 S_L(\Omega)$ with $S_L \simeq 2\hbar\omega_\gamma L$ for Poisson photon statistics.

Newtonian gravity-gradient (seismic/air). In the quasi-Newtonian limit,

$$S_\Phi^{\mathrm{N}}(\Omega) = (4\pi G)^2 \int \frac{d^3k}{(2\pi)^3} \frac{S_\rho(\boldsymbol{k},\Omega)}{k^4} |W(\boldsymbol{k})|^2, \tag{15}$$

which typically dominates at sub-Hz in ground laboratories. These components sum to $S_\Phi(\Omega)$ used in Eq. (8).

Hierarchy (order-of-magnitude). At $\sim$1 Hz in ground labs, seismic gravity-gradient noise typically implies $S_\Phi^{\mathrm{N}} \sim 10^{-32}\,\mathrm{s}$, whereas at $\sim$1 kHz the vacuum TT contribution is far smaller, $S_\Phi^{\mathrm{vac}} \sim 10^{-45}\,\mathrm{s}$; these site- and setup-dependent figures illustrate the practical dominance of Newtonian noise at low frequencies.

Appendix G: Units and conventions

Signature $(-,+,+,+)$, explicit c unless set to 1 in intermediate algebra. Areal radius r defined by $4\pi r^2$ equal to the area of symmetry spheres. Observer redshift factor ν_∞/ν_r defined as frequency ratio between asymptotic observer and local observer at radius r. Indices are raised/lowered with $g_{\mu\nu}$.

References

[1] Richard Arnowitt, Stanley Deser, and Charles W Misner. The dynamics of general relativity. *Annals of Physics*, 11(2):116–194, 1962.

[2] Adam Snyder. Gravity as temporal geometry: A quantizable reformulation of general relativity. Zenodo, 2024. URL `https://zenodo.org/records/16878019`. Paper I in the Time-First Gravity Series.

[3] Prahalad Chunnilal Vaidya. The gravitational field of a radiating star. *Proceedings of the Indian Academy of Sciences-Section A*, 33(5):264–276, 1951.

[4] Bei-Lok Hu and Enric Verdaguer. Stochastic gravity: theory and applications. *Living Reviews in Relativity*, 11(1):1–97, 2008.

[5] L. H. Ford. Spectrum of quantum fluctuations of stress-energy tensor. *Physical Review D*, 47 (12):5571–5580, 1993.

[6] Mark Kasevich and Steven Chu. Atomic interferometry using stimulated raman transitions. *Physical Review Letters*, 67(2):181–184, 1991.

[7] Andrew D Ludlow, Martin M Boyd, Jun Ye, Ekkehard Peik, and Piet O Schmidt. Optical atomic clocks. *Reviews of Modern Physics*, 87(2):637–701, 2015.

[8] Kyle Beloy, Martha I Bodine, Tobias Bothwell, Samuel M Brewer, Sarah L Bromley, Jwo-Sy Chen, Jean-Daniel Deschenes, Scott A Diddams, Robert J Fasano, Tara M Fortier, et al. Frequency ratio measurements at 18-digit accuracy using an optical clock network. *Nature*, 591 (7851):564–569, 2021.

[9] Markus Aspelmeyer, Tobias J Kippenberg, and Florian Marquardt. Cavity optomechanics. *Reviews of Modern Physics*, 86(4):1391–1452, 2014.

[10] Christian Lisdat, Gesine Grosche, Nils Quintin, Chunyan Shi, Sebastian M F Raupach, Christian Grebing, Daniele Nicolodi, Filippo Stefani, Ali Al-Masoudi, Sören Dörscher, et al. A clock network for geodesy. *Nature Communications*, 7(1):12443, 2016.

[11] T. Bothwell et al. Resolving the gravitational redshift across a millimetre-scale atomic sample. *Nature*, 602:420–424, 2022.

[12] S. M. Brewer et al. $^{27}al^{+}$ quantum-logic clock with systematic uncertainty of 9.4×10^{-19}. *Phys. Rev. Lett.*, 123:033201, 2019.

[13] R. Lange et al. Improved limits on the fine-structure constant variation using a yb^{+} clock. *Phys. Rev. Lett.*, 126:011102, 2021.

[14] S Al Kharusi et al. Snews 2.0: a next-generation supernova early warning system for multi-messenger astronomy era. *New Journal of Physics*, 23(3):031201, 2021.